



Lawrence Berkeley Laboratory

UNIVERSITY OF CALIFORNIA

CHEMICAL SCIENCES DIVISION

Submitted to Chemical Physics

The Ultraviolet Photodissociation Dynamics of Pyrrole

D.A. Blank, S.W. North, and Y.T. Lee

July 1994



REFERENCE COPY
Does Not
Circulate

Bldg. 50 Library.

LBL-35874

DISCLAIMER

This document was prepared as an account of work sponsored by the United States Government. While this document is believed to contain correct information, neither the United States Government nor any agency thereof, nor the Regents of the University of California, nor any of their employees, makes any warranty, express or implied, or assumes any legal responsibility for the accuracy, completeness, or usefulness of any information, apparatus, product, or process disclosed, or represents that its use would not infringe privately owned rights. Reference herein to any specific commercial product, process, or service by its trade name, trademark, manufacturer, or otherwise, does not necessarily constitute or imply its endorsement, recommendation, or favoring by the United States Government or any agency thereof, or the Regents of the University of California. The views and opinions of authors expressed herein do not necessarily state or reflect those of the United States Government or any agency thereof or the Regents of the University of California.

LBL-35874
UC-401

The Ultraviolet Photodissociation Dynamics of Pyrrole

David A. Blank, Simon W. North, and Yuan T. Lee

Department of Chemistry
University of California

and

Chemical Sciences Division
Lawrence Berkeley Laboratory
University of California
Berkeley, California 94720

July 1994

This work was supported by the Director, Office of Energy Research, Office of Basic Energy Sciences, Chemical Sciences Division, of the U.S. Department of Energy under Contract No. DE-AC03-76SF00098.

The Ultraviolet Photodissociation Dynamics of Pyrrole

David A. Blank, Simon W. North, Yuan T. Lee

*Chemical Sciences Division, Lawrence Berkeley Laboratory, and
Department of Chemistry, University of California, Berkeley,
California 94720*

Photofragment translational spectroscopy was used to study the photodissociation of pyrrole at 193 nm and 248 nm under collision-free conditions. Five primary dissociation channels were observed at 193 nm. Two channels resulted from cleavage of the N-H bond to yield H + pyrrolyl radical with one channel following internal conversion (IC) to the ground state (~21%) and the other originating from electronically excited pyrrole (~30%). Two dissociation channels involved elimination of HCN following IC. One channel producing HCN + vinylmethylene (~25%) following ring opening and hydrogen migration and the other proceeding via a bridged 3H-pyrrole intermediate to form HCN + cyclopropene (~24%). The last channel at 193 nm involved IC to the ground state followed by ring opening and N-C bond cleavage to form NH + CHCCHCH₂ (<1%). At 248 nm three dissociation channels were observed, all of which involved the elimination of atomic hydrogen. Analogous to the results at 193 nm, two of these channels resulted from cleavage of the N-H bond with one channel following IC (~42%) and the other dissociating from an excited electronic state (~47%). The third dissociation channel at 248 nm involved the cleavage of one of the two C-H bonds in electronically excited pyrrole (~11%). Translational energy distributions were determined for all observed dissociation channels. From consideration of the maximum translational energy of the photofragments $D_0(\text{N-H}) = 88 \pm 2$ kcal/mol, $D_0(\text{C-H}) = 112.5 \pm 1$ kcal/mol and $\Delta H_f(\text{pyrrolyl radical}) = 62 \pm 2$ kcal/mol were determined.

1. Introduction

Pyrroles and other nitrogen containing heterocyclic compounds serve as the main source of fuel nitrogen in coals and heavy-oils.¹ Eventhough the combustion of these compounds accounts for approximately 25% of all nitric oxide production, a component in air pollution of considerable concern, there have been few investigations concerning the combustion of pyrrole. The thermal decomposition of pyrrole has been studied by Lifshitz *et al.*² and Mackie *et al.*³ in two very

similar experiments using shock tube pyrolysis over temperature ranges of 1050-1450 K and 1200-1700 K respectively. Both studies found the major decomposition products to be HCN, methylacetylene, and acetylene with numerous other products appearing in smaller quantities. In both investigations the predominant decomposition pathway producing HCN and C₃H₄ was proposed to proceed via hydrogen migration and ring opening to the N=CH-CH=CH-CH₂ diradical which was followed by C-C bond cleavage.

Using photofragment translational spectroscopy (PTS) to study the photodissociation of pyrrole at 193 nm and 248 nm not only provides an opportunity to study dissociation pathways from electronically excited states of pyrrole, but where internal conversion (IC) to the electronic ground state precedes dissociation it allows investigation of *thermal decomposition of pyrrole under collision-free conditions*. In investigations of the photodissociation of the similar aromatic ring compounds cyclopentadiene⁴, thiophene⁴, benzene⁵, and pyridine⁶ at 193 nm the dissociations were found to proceed exclusively on the electronic ground state surface following IC from an initially excited Rydberg state. In the case of pyrrole we found only 70% of the dissociation events at 193 nm occurred on the ground electronic surface, the equivalent of thermal decomposition at 4040 K.⁷ At 248 nm only 42% of the dissociation events occurred on the ground electronic surface, the equivalent of thermal decomposition at 3320 K.⁷

Owing to the complicated nature of the electronic structure of pyrrole, assignment of the electronic spectrum has proven elusive in the face of extensive investigation. The UV absorption spectrum, which has an onset around 250 nm, has been measured by Mullen and Orloff⁸ and Bavia *et al.*⁹. The main features of the spectrum are a strong band with a maximum at 211 nm which Bavia *et al.* assigned to a Rydberg-like transition and a broad weak absorption centered around 237.5 nm which Mullen and Orloff attributed to a $\pi \rightarrow \pi^*$ transition corresponding to the first excited singlet state. The most successful assignment of the electronic spectrum of pyrrole has come from the recent work of Serrano-Andres *et al.*¹⁰ using detailed ab initio calculations. They found two Rydberg series, $1a_2 \rightarrow 3n$ and $2b_1 \rightarrow 3n$, underlying two strong features at 6.0 eV and 7.5 eV which were attributed to the valence excited states 2^1B_2 and 6^1A_1 respectively. The feature at 5.08 eV was assigned to the first Rydberg series, $1^1A_2 (1a_2 \rightarrow 3s)$, and the five

components of the $1a_2 \rightarrow 3d$ series were found between 6.40 eV and 6.54 eV with only the 3^1B_1 at 6.40 eV having significant intensity. Based on the work of Serrano-Andres *et al.* the excitation at 193 nm (6.4 eV) is predominantly a transition to the $3^1B_1(1a_2 \rightarrow 3d)$ Rydberg state and the excitation at 248 nm (5.0 eV) is predominantly a transition to the $1^1A_2(1a_2 \rightarrow 3s)$ Rydberg state.

We have investigated the photodissociation of pyrrole at 193 nm and 248 nm using PTS. At 193 nm we have identified five primary dissociation channels, one involving elimination of atomic hydrogen from an excited electronic state and the other four dissociating from the electronic ground state following IC. The dissociations from the electronic ground state include elimination of atomic hydrogen, two pathways yielding HCN, and the elimination of NH. At 248 nm we have identified three primary dissociation channels, all of which involve elimination of atomic hydrogen. Two of these channels are dissociations from excited electronic states and one dissociation proceeds via the electronic ground state following IC. The translational energy distributions of the photofragments and the branching ratios have been determined for all primary dissociation channels.

2. Experimental

The rotatable-source/fixed-detector experimental apparatus, figure 1(a), has been described in detail elsewhere.¹¹ Briefly, 70 torr of 7% pyrrole seeded in He was expanded through a 0.375 mm diameter nozzle into a source chamber maintained at 5×10^{-4} torr. The nozzle was heated to 70°C to inhibit dimer formation and the resulting average beam velocity was 1300 m/s with a FWHM of 10%. The beam was collimated twice and subsequently intersected with the output of a Lambda Physik EMG103MSC eximer laser operating on the ArF (193 nm) and KrF (248 nm) transitions. The laser was focused to a 2 x 4 mm spot in the interaction region with fluence ranging 1 - 100 mJ/cm². For laser polarization measurements the laser polarization was rotated using ten quartz plates at Brewster's angle to provide 95% polarized light.

Photofragments recoiling out of the beam traveled 36.7 cm where they were ionized using electron bombardment, mass selected with a quadrupole mass filter, and counted with a Daly ion counter.¹² Time-of-flight (TOF) spectra were collected using a multichannel scaler with a bin

width of 1-2 μs . The ability of the source to rotate about the axis of the laser enabled TOF spectra to be taken at multiple angles with respect to the detector. Center of mass translational energy distributions were determined using the forward convolution technique.¹³

For the detection of $m/e = 1 - 2$ photofragments the experimental setup was modified as shown in figure 1(b). A pulsed molecular beam source was used to expand 100 torr of 1% pyrrole seeded in He into a source region maintained at 5×10^{-5} torr. The beam was photolyzed 0.5 cm above the nozzle in the source region, and those photofragments which recoiled 90° out of the beam traveled 28.4 cm, passing through two defining apertures, and were detected by the same method described above. The molecular beam, laser, and detector were all mutually perpendicular. TOF spectra were collected using a multichannel scaler with a bin width of 0.5 μs . Laser fluence ranged 10 - 1000 mJ/cm^2 .

Pyrrole, 98%, was obtained from Aldrich Chemical Company and used without further purification. Pyrrole- d_4 , 98%, was obtained from Cambridge Isotopes and used without further purification. Isotopic purity of d_4 -pyrrole was verified by ^{13}C NMR.

3. Results

All primary product channels reported exhibited linear dependence on the laser fluence indicating that the dissociations are single photon events. For all TOF spectra presented, the open circles represent the data, the solid lines are the overall fits to the data, and the dashed lines represent individual contributions to the data from separate product channels. The angle for each TOF spectrum refers to the angle of the molecular beam with respect to the detector axis. Only a fraction of the TOF spectra used in determination of translational energy distributions have been presented.

3.1 Photodissociation at 193 nm. At 193 nm primary dissociation products were identified at $m/e = 1, 15, 27, 40, 52,$ and 66. TOF spectra were taken at multiple source angles with respect to the detector in order to improve the confidence of the forward convolution fits and to discriminate between separate product channels which may be detected at the same m/e ratio due

to dissociative ionization of products at higher masses (see the Newton diagram in figure 2).

3.1.1 Elimination of atomic hydrogen. TOF spectra for $m/e = 1$ (H^+) at 90° for both pyrrole and d_4 -pyrrole are shown in figure 3, and the TOF spectra for the momentum matched fragments at $m/e = 66$ ($C_4H_4N^+$) for non-deuterated pyrrole are shown in figure 4 at source angles of 4° and 10° . The $m/e = 1$ TOF spectrum for non-deuterated pyrrole shows two separate contributions, one faster sharp contribution peaked at $22 \mu s$, and one slower broad contribution which extends out to $100 \mu s$. The center of mass (c.o.m.) translational energy distributions, $P(E_t)$, used to fit the data in figures 3 and 4 are shown in figure 5. The faster channel was fit with a translational energy distribution peaked at 22 kcal/mol and extending to a maximum of 60 kcal/mol (represented by the filled circles in figure 5). The slow broad channel was fit with the $P(E_t)$ peaked at 2.5 kcal/mol and exponentially decreasing to a maximum of 60 kcal/mol (represented by the filled triangles in figure 5). The fits to the data at $m/e = 66$ using the translational energy distributions in figure 5 confirm the $m/e = 66$ products are the momentum matched photofragments to the two $m/e = 1$ products. The d_4 -pyrrole spectrum in figure 3 shows both of the hydrogen atom loss channels observed in the non-deuterated pyrrole spectrum. This and the failure to detect any $m/e = 2$ (D^+) products from d_4 -pyrrole after one million laser shots establishes that both of the observed atomic hydrogen elimination channels were the result of N-H bond cleavage.

Assuming the maximum translational energy release, 60 kcal/mol for both hydrogen elimination channels, corresponds to internally cold products, the N-H bond dissociation energy can be calculated as the difference between the photon energy and the maximum translational energy:

$$D_o(N-H) = E_{hv(193 \text{ nm})} - P(E_t)_{\max} = 148 \text{ kcal/mol} - 60 \text{ kcal/mol} = 88 \pm 2 \text{ kcal/mol}$$

This calculation of the bond dissociation energy assumes no initial excitation in the parent molecule prior to dissociation, which is a reasonable assumption considering pyrrole at $70^\circ C$ contains 1.2 kcal/mol of vibrational energy and should experience substantial relaxation upon expansion. The N-H dissociation energy is consistent with the formation of ground state pyrrolyl radical and hydrogen atom products providing a direct measurement of the N-H bond energy.

Uncertainty in the value of $D_0(\text{N-H})$ was ± 2 kcal/mol based on the sensitivity of the forward convolution fit to $P(E_t)_{\text{max}}$. Using this bond energy and the known heats of formation for pyrrole and atomic hydrogen $\Delta H_f(\text{pyrrolyl radical}) = 62 \pm 2$ kcal/mol.

3.1.2 Elimination of HCN. The TOF spectra for $m/e = 27$ (HCN^+) are shown in figure 6 for source angles of 10° and 25° . At 10° the spectrum has been fit with four contributions, the faster two components represent primary product channels resulting in $m/e = 27$ photofragments, and the slower two contributions are the result of $m/e = 66$ ($\text{C}_4\text{H}_4\text{N}^+$) photofragments cracking in the ionizer to $m/e = 27$. The $m/e = 66$ photofragments have insufficient energy to recoil out beyond 15° (see Newton diagram in figure 2) leaving only two $m/e = 27$ contributions to the TOF at 25° . The momentum matched partners to the two $m/e = 27$ photofragments were found at $m/e = 40$ (C_3H_4^+). Due to enhanced signal to noise, the $m/e = 40$ products were monitored at the daughter ion $m/e = 39$ (C_3H_3^+) and the TOF spectra for $m/e = 39$ at 25° and 35° are shown in figure 7. The $P(E_t)$ used to fit both of the $\text{HCN} + \text{C}_3\text{H}_4$ channels are shown in figure 8. The faster HCN elimination channel, peaked at $110 \mu\text{s}$ in the $m/e = 27$ spectrum, and its momentum matched fragment at $160 \mu\text{s}$ in the $m/e = 39$ spectrum, were fit with the $P(E_t)$ in figure 8 which peaks at 21 kcal/mol and extends out to a maximum of 68 kcal/mol (represented by the filled circles in figure 8). The slower broad feature was fit with a $P(E_t)$ peaked near zero kcal/mol and extending to a limit of 25 kcal/mol (represented by the filled triangles in figure 8).

3.1.3 Elimination of NH. The final primary product channel found at 193 nm resulted in $m/e = 15$ (NH^+) + $m/e = 52$ (C_4H_4^+). This channel minor comprised $< 1\%$ of the total dissociation yield at 193 nm (see section 3.4). TOF spectra for $m/e = 15$ at 15° and 20° are shown in figure 9 and the TOF spectra for $m/e = 52$ at 12° and 17.8° are shown in figure 10. In the $m/e = 15$ TOF spectra the slow broad feature represents the primary $m/e = 15$ photoproduct and the two faster features are the result of higher mass photofragments from one of the $m/e = 27 + m/e = 40$ channels cracking in the ionizer to $m/e = 15$. The $m/e = 52$ spectrum at 12° shows a small contribution peaked at $290 \mu\text{s}$ from the $m/e = 66$ primary product channel, and at 17.8° the only feature remaining in the spectrum was the $m/e = 52$ product. The $P(E_t)$ used to fit the $m/e = 15 + m/e = 52$ contribution to the TOF spectra in figures 9 and 10 is shown in figure 11. The $P(E_t)$ is

peaked near zero kcal/mol and decreases exponentially to a limit of 17 kcal/mol.

3.2 Photodissociation at 248 nm. At 248 nm three primary product channels were identified, all of which involved elimination of atomic hydrogen. Figure 12 shows the TOF spectra for $m/e = 1$ (H^+) at 90° for non-deuterated and d_4 -pyrrole and figure 13 shows the TOF spectra for the momentum matched $m/e = 66$ ($C_4H_4N^+$) photofragments at 5° and 8° . There were three features in the $m/e = 1$ spectrum for non-deuterated pyrrole, a fast sharp feature peaked at 24 μsec , a very broad contribution extending from 18 μsec to 100 μsec , and a slow peak centered at 72 μsec . The $m/e = 1$ spectrum for d_4 -pyrrole exhibited both of the first two peaks but was missing the slow peak indicating that the slow peak originated from C-H bond cleavage and the first two peaks were the result of N-H bond cleavage. The d_4 -pyrrole $m/e = 1$ spectrum was taken with a laser fluence of 500 mJ/cm^2 in order to enhance signal to noise. At this laser fluence multiphoton processes were found to enhance the intensity of the slow broad peak slightly in comparison to the non-deuterated spectrum taken in a linear regime (20 mJ/cm^2). However, the slow contribution at 72 μsec was clearly absent from the d_4 -spectrum even at higher laser fluence.

The $m/e = 66$ spectra exhibit contributions from both of the faster channels. The slow channel from C-H bond cleavage could not be seen in the $m/e = 66$ spectra since it is not kinematically possible for it to recoil out to 5° . TOF spectra at angles $< 5^\circ$ were not taken due to large background from the molecular beam. The $P(E_t)$ used to fit the two faster channels which result from N-H bond cleavage are shown in figure 14(a). The sharp narrow channel peaked at 24 μsec in the $m/e = 1$ spectrum was fit with the $P(E_t)$ peaked at 17 kcal/mol and extending to a maximum of 27 kcal/mol (represented by the filled circles in figure 14a). The broad peak was fit with the $P(E_t)$ peaked at 2.5 kcal/mol and extending to 27 kcal/mol (represented by the filled triangles in figure 14a). The slow channel at 72 μsec in the $m/e = 1$ spectrum which resulted from C-H bond cleavage was fit with the $P(E_t)$ in figure 14(b) peaked at 1.7 kcal/mol and extending to 2.7 kcal/mol.

Bond dissociation energies were obtained as described in section 3.1.1. The $P(E_t)_{\text{max}}$ for both of the N-H bond cleavage channels was 27 ± 2 kcal/mol giving a value for $D_0(\text{N-H})$ of 88 ± 2 kcal/mol, which agrees extremely well with the value obtained from the data at 193 nm. For the C-H bond dissociation channel the $P(E_t)_{\text{max}}$ was 2.7 ± 1 kcal/mol resulting in a value of $D_0(\text{C-H}) =$

112.3±1 kcal/mol.

3.3 Polarization dependence at 193 nm and 248 nm. The signal intensity for the fast atomic hydrogen loss channel was measured at $m/e = 66$ as a function of the laser polarization angle at both 193 nm and 248 nm. At 193 nm the data was taken at a source angle of 11° and at 248 nm at a source angle of 8° . The source angles were chosen in order to minimize the contribution from the ground state H-atom elimination channel while maintaining an acceptable signal to noise ratio. Figure 15 shows the plots of intensity versus the laser polarization angle corrected to the center of mass for 193 nm, fig. 15(a), and 248 nm, fig. 15(b). The data was fit according to $P(\theta) = 1 + \beta P_2(\cos\theta)^{14}$ where β ranges -1 to 2. The best fit to the 193 nm data was obtained with $\beta = 0.27 \pm 0.03$ and at 248 nm the best fit to the data was found with $\beta = 0.33 \pm 0.02$. These β values represent a lower limit since at a given laboratory angle of the source with respect to the detector one measures a finite spread of c.o.m. angles (see figure 2) and this spread in the c.o.m. angles results in a lower measured β . In both cases the measurement of a positive β indicates that the transition dipole has a component that lies parallel to dissociation coordinate.

3.4. Estimation of product branching ratios at 193 nm and 248 nm. The branching ratios are reported in table 1. The branching ratios at 193 nm were calculated as described in reference 15 according to equation 1 where σ_a^o and σ_b^o are the relative cross sections of fragments a and b

$$\frac{\sigma_a^o}{\sigma_b^o} \times \frac{Q_b}{Q_a} \times \frac{F_b}{F_a} = \frac{\sigma_a}{\sigma_b} = R$$

monitored at a given m/e ratio and corrected for kinematics. Q_a and Q_b are the ionization cross sections of the products which result in fragments a and b and were calculated using the method of Fitch and Sauter.¹⁶ F_a and F_b are the probabilities of the products cracking in the ionizer to form fragments a and b at the given m/e ratio. We estimate the uncertainty in the branching ratios obtained in this way to be $\pm 25\%$.

At 248 nm the production of atomic hydrogen in all three product channels greatly simplified the branching ratio calculations since the hydrogen atom product only appears at one m/e ratio and there is no difference in the ionization cross sections. Therefore, the branching ratios could be obtained directly from the fit to the $m/e = 1$ TOF spectrum. The uncertainty in the branching ratios at 248 nm was limited only by the fit to the $m/e = 1$ data which we estimate to be

±10%.

4. Discussion

4.1 Photodissociation at 193 nm.

4.1.1 H-atom elimination channels. Since both H-atom elimination channels resulted from N-H bond cleavage and both lead to the same asymptotic products, the two dissociations most likely occur on different electronic surfaces. The slow H-atom channel has a $P(E_t)$ peaked at 2.5 kcal/mol and exponentially decreasing with only 15% of the available energy released in translation on average, $\langle E_t \rangle = 9$ kcal/mol. This type of translational energy distribution, peaked near zero and exponentially decreasing, is representative of a statistical dissociation involving simple bond rupture to form two radical products. If one assumes an RRKM type $P(E_t)$ at the transition state where the maximum in the measured $P(E_t)$ represents conversion of all of the potential energy into translation while descending from the transition state along the reaction coordinate, the maximum in the measured $P(E_t)$ would provide the height of the dissociation barrier. If any of the potential energy is converted to internal energy of the products while descending from the transition state, the maximum in the measured $P(E_t)$ would be shifted to lower energy. The maximum in the measured $P(E_t)$ can thus be considered as a lower limit to the dissociation barrier. Therefore the slow channel occurs on the electronic ground state following internal conversion over a barrier with a lower limit of 2.5 kcal/mol. The barrier in this process results from the electronic rearrangement of the ring in going from pyrrole to the pyrrolyl radical. In comparison the analogous H-atom loss in cyclopentadiene was found to have barrier with a lower limit of 5 kcal/mol.⁴ The higher barrier reflects a more extensive electronic rearrangement involving movement of the remaining hydrogen on the methylene group into the plane of the molecule.

With the slow channel occurring on the ground state surface it is probable that the fast H-atom elimination occurs on an electronic excited surface. Owing to the lack of available information concerning the excited state surfaces of pyrrole it is not possible to assign the excited state involved in the dissociation. Assuming the initial excitation to involve excitation to the 3d Rydberg state which is not dissociative, a surface crossing from the initial 3d Rydberg to the involved dissociative surface must occur rapidly compared with rotation of the pyrrole molecule

in order to exhibit the measured anisotropy. In order for IC to be competitive with this process the initial IC must also be rapid, most likely involving crossing to a lower lying Rydberg state, with subsequent IC leading to the ground electronic surface. This is consistent with the rapid IC found between excited electronic states in most aromatic hydrocarbons.¹⁷ An alternative explanation consistent with the competing H-atom elimination channels would be that the initial excitation is to overlapping Rydberg and dissociative excited states. Both explanations are supported by the data and without additional information we are unable to discriminate between the two. It is interesting to note that although at 193 nm cyclopentadiene⁴, thiophene⁴, benzene⁵, and pyridine⁶ all involve an analogous initial Rydberg excitation, dissociation in all four cases proceeds exclusively on the ground electronic surface following IC. No excited state dissociation channels were observed at 193 nm for any of these four compounds demonstrating a fundamental difference between their electronic structure and that of pyrrole.

4.1.2 HCN elimination channels. The $P(E_t)$ for the slow HCN elimination channel, peaked near zero and exponentially decreasing, reflects a dissociation involving simple bond rupture. This channel therefore proceeds via an initial opening of the pyrrole ring and hydrogen migration to form the $N=CH-CH=CH-CH_2$ diradical. The hydrogen migration has been hypothesized to either occur prior to ring opening forming 2H-pyrrole followed by C-N bond cleavage³ or to occur concurrently with ring opening in a concerted mechanism². A rough estimation of the energy required to form the diradical was obtained using MOPAC¹⁸ to calculate the ΔH_f of the diradical which was found to be 65 kcal/mol unstable with respect to pyrrole. Once the ring is open the C-C bond is broken in a near barrierless process to form HCN and vinylmethylene. From the $P(E_t)_{max}$ of 25 ± 5 kcal/mol for this process and the known ΔH_f for HCN¹⁹ and pyrrole²⁰ we calculate this dissociation to be 123 ± 5 kcal/mol endothermic. Yoshimine *et al.*²¹ have calculated the stability of vinylmethylene with respect to methylacetylene to be 45.9 kcal/mol for the triplet, 62.7 kcal/mol and 60.2 kcal/mol for the singlet diradical and singlet carbene respectively. This leads to dissociation energies of 94 kcal/mol for the triplet, 111 kcal/mol for the singlet diradical, and 109 kcal/mol for the singlet carbene forms of vinylmethylene. Based on these values our results are most consistent with formation of singlet vinylmethylene with the energy difference between the carbene and diradical too small to allow any distinction.

The fast HCN elimination channel had a $P(E_t)_{\max}$ of 68 ± 2 kcal/mol leading to a measured dissociation energy of 80 ± 2 kcal/mol. This is in excellent agreement with the dissociation energy of 80 kcal/mol calculated for the production of HCN + cyclopropene from the well know heats of formation for pyrrole²⁰, HCN¹⁹ and cyclopropene²². The $P(E_t)$ is peaked well away from zero at 21 kcal/mol indicating a concerted mechanism whereby HCN elimination occurs with high average translational energy, $\langle E_t \rangle = 26$ kcal/mol, resulting from the formation of two closed shell products in very close proximity. The only other thermodynamically available C_3H_4 products are allene and methylacetylene, both of which are >20 kcal/mol more stable than cyclopropene²¹, energy which cannot be accounted for based on the measured $P(E_t)$ and thus confirming cyclopropene as the identity of the C_3H_4 product.

We propose the following dissociation mechanism for the formation of HCN + cyclopropene (see far left of figure 16). The first step is hydrogen migration to form 3H-pyrrole. Calculations on 1,5 sigmatropic hydrogen shifts in pyrrole by Bachrach²³ show the initial 1,5 H-atom shift to form 2H-pyrrole to be 13.0 kcal/mol endothermic with a barrier of 44.5 kcal/mol and the subsequent 1,5 H-atom shift to form 3H-pyrrole to be endothermic by an additional 2.1 kcal/mol with a barrier of 39.3 kcal/mol with respect to pyrrole. Next, the 3H-pyrrole isomerizes to form the bridged 3H-pyrrole which we have roughly estimated to lie 66 kcal/mol above pyrrole using MOPAC¹⁸. Although the bridged form of 3H-pyrrole has not been investigated to our knowledge, the analogous bridged structure, 5-azabicyclo[2.1.0]pent-2-ene, has been identified by Barltrop *et al.*²⁴ as the intermediate in the UV photoisomerization of 2-cyanopyrrole to 3-cyanopyrrole. From the bridged 3H-pyrrole, cleavage of two C-C bonds results in the concerted elimination of HCN and cyclopropene.

The shock tube pyrolysis studies^{2,3} found the major decomposition products to be HCN and methylacetylene. This is consistent with our results if one considers the thermal isomerization of cyclopropene to allene and methylacetylene. The isomerization to methylacetylene has been determined to be the faster process with experimental activation energies²⁵ of 43.3 kcal/mol for cyclopropene \rightarrow allene and 37.5 kcal/mol for cyclopropene \rightarrow methylacetylene. Theoretical studies²¹ have identified the intermediates in the C_3H_4 isomerization to be vinylmethylene between cyclopropene and allene and propenylidene between cyclopropene and methylacetylene.

Therefore the continued pyrolysis of the primary C₃H₄ products, cyclopropene and vinylmethylene, is expected to result predominantly in the production of methylacetylene along with a small yield of allene providing very good agreement with the pyrolysis experiments.

4.1.3 NH elimination channel. The shape of the P(E_v) indicates simple bond rupture with the maximum in the P(E_v), P(E_v)_{max} = 17±2 kcal/mol, providing a dissociation energy of 131±2 kcal/mol. This is in excellent agreement with the dissociation energy of 130±2 kcal/mol to form NH + CH₂=C-CH=CH₂ calculated from the experimental ΔH_f for NH²⁶ and pyrrole²⁰, and using group additivity²⁷ to estimate ΔH_f for CH₂=C-CH=CH₂. This dissociation channel involves direct opening of the pyrrole ring to form the NH-CH=CH-CH=CH diradical, which we roughly estimate to be 80 kcal/mol endothermic from a MOPAC¹⁸ calculation, followed by cleavage of the N-C bond. The peak in the P(E_v) near zero kcal/mol (note that the P(E_v) was not determined below 3 kcal/mol for this channel due to kinematic considerations) shows this dissociation to proceed over little or no barrier. The only other thermodynamically possible C₄H₄ product at 193 nm is CH₂=C=C=CH₂ which leads to a calculated dissociation energy of 136±2 kcal/mol and can thus be ruled out based on the measured P(E_v)_{max}.

4.2 Photodissociation at 248 nm. At 248 nm we found three hydrogen elimination channels, two involving N-H bond cleavage and one resulting from C-H bond cleavage. The two N-H bond dissociation channels are directly analogous to the two H-atom elimination channels at 193 nm. The slow H-atom channel is a thermal dissociation from the ground electronic state and the fast channel involves dissociation on an excited electronic surface. In both cases the asymptotic products are the pyrrolyl radical and atomic hydrogen. The P(E_v) for the slow channel is peaked at 2.5 kcal/mol confirming the lower limit to the barrier for the ground state dissociation determined at 193 nm. The fast channel has a P(E_v) peaked well away from zero and exhibits similar anisotropy to that found at 193 nm. The measured β of 0.33±0.02 indicates either a rapid crossing from the initial Rydberg state to the electronic surface upon which the dissociation occurs or an initial excitation to overlapping Rydberg and dissociative surfaces.

The absence of the C-H bond cleavage channel at 193 nm and the fact that it accounts for 11% of the dissociation at 248 nm while being 24 kcal/mol less energetically favorable than the other two channels means that this dissociation does not occur on the ground electronic surface. If

this were a ground state dissociation competing with the ground state N-H dissociation where the barrier is more than 22 kcal/mol lower, we would not expect the yield to be nearly as significant as 11%. Without additional information on the electronic structure of pyrrole we are unable to identify the electronic surface(s) involved. Additional evidence of an excited state dissociation would have been provided by measurement of a non-zero β parameter, unfortunately low signal/noise prevented us from performing laser polarization measurements on this channel.

5. Conclusion

Figure 16 is a summary of the photodissociation of pyrrole at 193 nm and 248 nm including proposed intermediates in the dissociation pathways. At 193 nm we observed five competing dissociation channels. One of these channels involved dissociation of the N-H bond from an excited electronic state to form the pyrrolyl radical and atomic hydrogen, and the four other dissociation channels occurred on the electronic ground state, the equivalent of thermal decomposition at 4040 K. The ground state dissociations included (1) cleavage of the N-H bond to give the pyrrolyl radical and atomic hydrogen over a barrier of 2.5 kcal/mol, (2) opening of the pyrrole ring with hydrogen migration followed by dissociation to yield HCN and vinylmethylene, (3) a concerted elimination involving a bridged 3H-pyrrole intermediate to yield translationally hot HCN and cyclopropene, and (4) direct opening of the pyrrole ring followed by dissociation of the N-C bond to give NH and $\text{CH}\equiv\text{C}-\text{CH}=\text{CH}_2$. The thermal dissociations which resulted in the production of HCN and C_3H_4 were found to be consistent with previous pyrolysis experiments. From the maximum in the translational energy distributions for the two N-H bond dissociation channel, $D_0(\text{N-H})$ was determined to be 88 ± 2 kcal/mol.

At 248 nm we observed three competing dissociation channels, all of which resulted in the elimination of atomic hydrogen. Analogous to the two H-atom elimination channels at 193 nm there were two channels involving cleavage of the N-H bond to yield the pyrrolyl radical and atomic hydrogen. One of the N-H bond dissociations occurred on the electronic ground state, the equivalent of thermal dissociation at 3320 K, and the other dissociating from an excited electronic state. The third dissociation channel at 248 nm was not observed at 193 nm and involved C-H bond cleavage from an excited electronic state. From consideration of $P(E_t)_{\text{max}}$, $D_0(\text{C-H})$ was determined to be 112.3 ± 1 kcal/mol.

Although the ground state dissociations are consistent with previous pyrolysis experiments, the observed excited state dissociations are somewhat surprising in light of the UV dissociation behavior of the similar aromatic ring compounds cyclopentadiene⁴, thiophene⁴, benzene⁵, and pyridine⁶ where the dissociations all occur exclusively on the ground electronic surface following IC from an initial Rydberg excitation. The complex UV dissociation behavior exhibited by pyrrole reflects the fact that its electronic structure is complicated and distinct from that of other similar heterocyclic aromatic compounds.

Acknowledgments. The authors would like to thank Dr. A. Suits for helpful discussions. D.B. would like to thank Dr. J. D. Myers for helpful discussions. This work was supported by the Director, Office of Energy Research, Office of Basic Energy Sciences, Chemical Sciences Division of the U.S. Department of Energy under contract No. DE-AC03-76SF00098 and The Office of Naval Research.

References.

1. R. L. Snyder, B. E. Buell, H. E. Howard, *Anal. Chem.* **40**, 1303 (1968). L. R. Snyder, *Anal. Chem.* **41**, 314 (1969). A. E. Axworthy, V. H. Dayan, G. B. Martin, *Fuel* **57**, 29 (1978). P. R. Solomon, M. B. Colket, *Fuel* **57**, 749 (1978). P. C. Painter, M. M. Coleman, *Fuel* **58**, 301 (1979).
2. A. Lifshitz, C. Tamburu, A. Suslensky, *J. Phys. Chem.* **93**, 5802 (1989).
3. J. C. Mackie, M. B. Colket, P. F. Nelson, *J. Phys. Chem.* **94**, 4099 (1990).
4. J. D. Myers, Ph.D. thesis, University of California, Berkeley, (1993).
5. A. Yokoyama, X. Zhao, E. J. Hints, R. E. Continetti, Y. T. Lee, *J. Chem. Phys.* **92**, 4222 (1990).
6. K. A. Prather, Y. T. Lee (unpublished results)
7. Thermal temperatures were calculated based on the experimental vibrational frequencies of pyrrole determined by J. S. Hutchinson, J. T. Hynes, W. P. Reinhart, *J. Phys. Chem.* **90**, 3528 (1986).
8. P. A. Mullen, M. K. Orloff, *J. Chem. Phys.* **51**, 2276 (1969).
9. M. Bavia, F. Bertinelli, C. Taliani, C. Zauli, *Mol. Phys.* **31**, 479 (1976).
10. L. Serrano-Andres, M. Merchan, I. Nebot-Gil, B. O. Roos, M. Fulscher, *J. Am. Chem. Soc.* **115**, 6184 (1993).
11. A. M. Wodtke, Y. T. Lee, *J. Phys. Chem.* **89**, 4744 (1985).
12. Y. T. Lee, J. D. McDonald, P. R. LeBreton, D. R. Herschbach, *Rev. Sci. Instrum.* **40**, 1402 (1969).
13. A. M. Wodtke, Ph.D. thesis, University of California, Berkeley, (1986); X. Zhao, Ph.D. thesis, University of California, Berkeley, (1988).
14. R. N. Zare, *Mol. Photochem.* **4**, 1 (1974).
15. A. M. Schmoltner, Ph.D. thesis, University of California, Berkeley, (1989).
16. W. L. Fitch, A. D. Sauter, *Anal. Chem.* **55**, 832 (1983).
17. N. J. Turro, *Modern Molecular Photochemistry*, The Benjamin/Cummings Publishing

- Company, Inc., Menlo Park, California, (1978).
18. MOPAC v.6.0 computational chemistry package, James J. P. Stewart, Frank J. Seiler Research Laboratory, United States Air Force Academy, 1990.
 19. JANAF Interim Thermochemical Tables, D. R. Stull Ed., Dow Chemical Co., Midland, Mich., 1960-1966.
 20. D. W. Scott, W. T. Berg, I. A. Hossenlopp, W. N. Hubbard, J. F. Messerley, S. S. Todd, D. R. Douslin, J. P. McCullough, G. Waddington, G. J. Phys. Chem. **71**, 2263 (1967).
 21. M. Yoshimine, J. Pacansky, N. Honjou, J. Am. Chem. Soc. **111**, 4198 (1989).
 22. K. B. Wilberg et al., J. Am. Chem. Soc. **84**, 3980 (1962).
 23. S. M. Bachrach, J. Org. Chem. **58**, 5414 (1993).
 24. J. A. Barltrop, A. C. Day, R. W. Ward, J.C.S. Chem. Comm. 131 (1978).
 25. I. M. Baily, R. Walsh, J. Chem. Soc. Faraday Trans. I **74**, 1146 (1978).
 26. S. T. Gibson, J. P. Green, J. Berkowitz, J. Chem. Phys. **83**, 4319 (1985).
 27. S. W. Benson, *Thermochemical Kinetics*, 2nd ed., Wiley, New York, (1976).

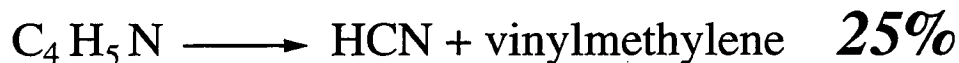
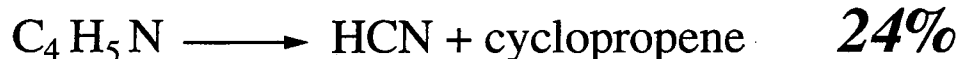
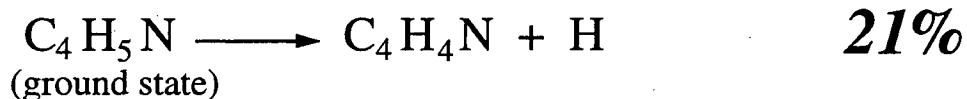
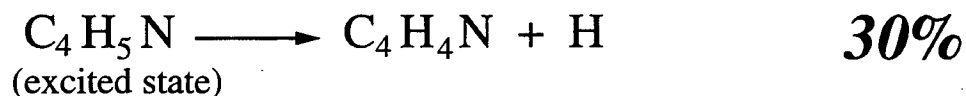
Figure Captions.

- Figure 1.** The experimental configuration. (a) The rotatable source/fixed detector configuration for detection of $m/e = 12-66$ photofragments. (b) The configuration for detection of $m/e = 1-2$ photofragments. *In both figures:* 1. The molecular beam source. 2. The molecular beam. 3. Detected recoiling photofragments. 4. UV laser (propagation orthogonal to the page). 5. The detector.
- Figure 2.** Newton diagram for the photodissociation of pyrrole at 193 nm. The circles represent the thermodynamic limit for each photofragment.
- Figure 3.** TOF spectra at 193 nm for $m/e = 1$ (H^+) at 90° for (a) non-deuterated pyrrole and (b) d_4 -pyrrole. The circles represent the data. The broken lines represent contributions from individual product channels and the solid line represents the overall fit to the data.
- Figure 4.** Same as figure 3 for $m/e = 66$ ($C_4H_4N^+$) at (a) 4° and (b) 10° .
- Figure 5.** Center of mass translational energy distributions for the two atomic hydrogen elimination channels. The filled triangles represent the distribution for the slow channel. The filled circles represent the distribution for the fast channel.
- Figure 6.** Same as figure 3 for $m/e = 27$ at (a) 10° and (b) 25° .
- Figure 7.** Same as figure 3 for $m/e = 39$ at (a) 25° and (b) 35° .
- Figure 8.** Center of mass translational energy distributions for the two HCN elimination channels. The filled triangles represent the distribution for the dissociation for the formation of HCN + vinylmethylene. The filled circles represent the distribution for the formation of HCN + cyclopropene.
- Figure 9.** Same as figure 3 for $m/e = 15$ at (a) 15° and (b) 20° .
- Figure 10.** Same as figure 3 for $m/e = 52$ at (a) 12° and (b) 17.8° .
- Figure 11.** Center of mass translational energy distribution for the NH elimination channel.
- Figure 12.** TOF spectra at 248 nm for $m/e = 1$ (H^+) at 90° for (a) non-deuterated pyrrole and (b) d_4 -pyrrole. The circles represent the data. The broken lines represent contributions from individual product channels and the solid lines represents the overall fit to the data.

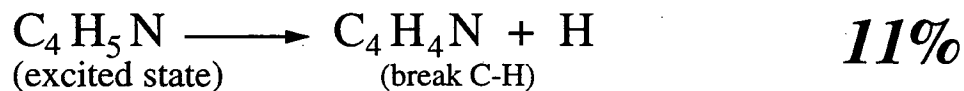
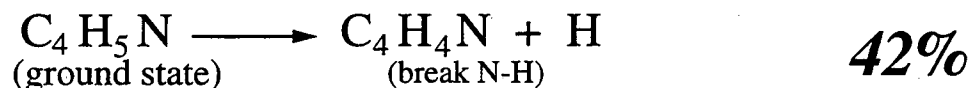
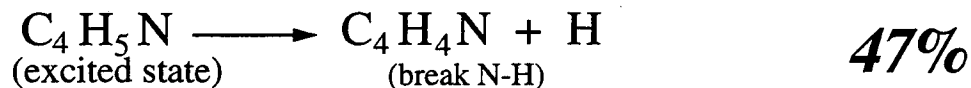
- Figure 13.** Same as figure 12 for $m/e = 66$ ($C_4H_4N^+$) at (a) 5° and (b) 8° .
- Figure 14.** Center of mass translational energy distributions for the three atomic hydrogen elimination channels. (a) Dissociations involving N-H bond cleavage. The filled triangles represent the distribution for the dissociation from the electronic ground state. The filled circles represent the distribution for the dissociation from an excited electronic state. (b) The dissociation involving C-H bond cleavage.
- Figure 15.** Center of mass laser polarization dependence for the fast $m/e = 66$ ($C_4H_4N^+$) channel. The points are the data, the lines represent the best fit to the data. (a) 193 nm with the data taken at a source angle of 11° . The best fit to the data represents $\beta = 0.27 \pm 0.03$. (b) 248 nm with the data taken at a source angle of 8° . The best fit to the data represents $\beta = 0.33 \pm 0.02$.
- Figure 16.** Summary of all observed photodissociation channels. Energies are relative to pyrrole. Origin of thermodynamic values and branching ratios are explained in the text.

Table 1. Branching Ratios.

193 nm



248 nm



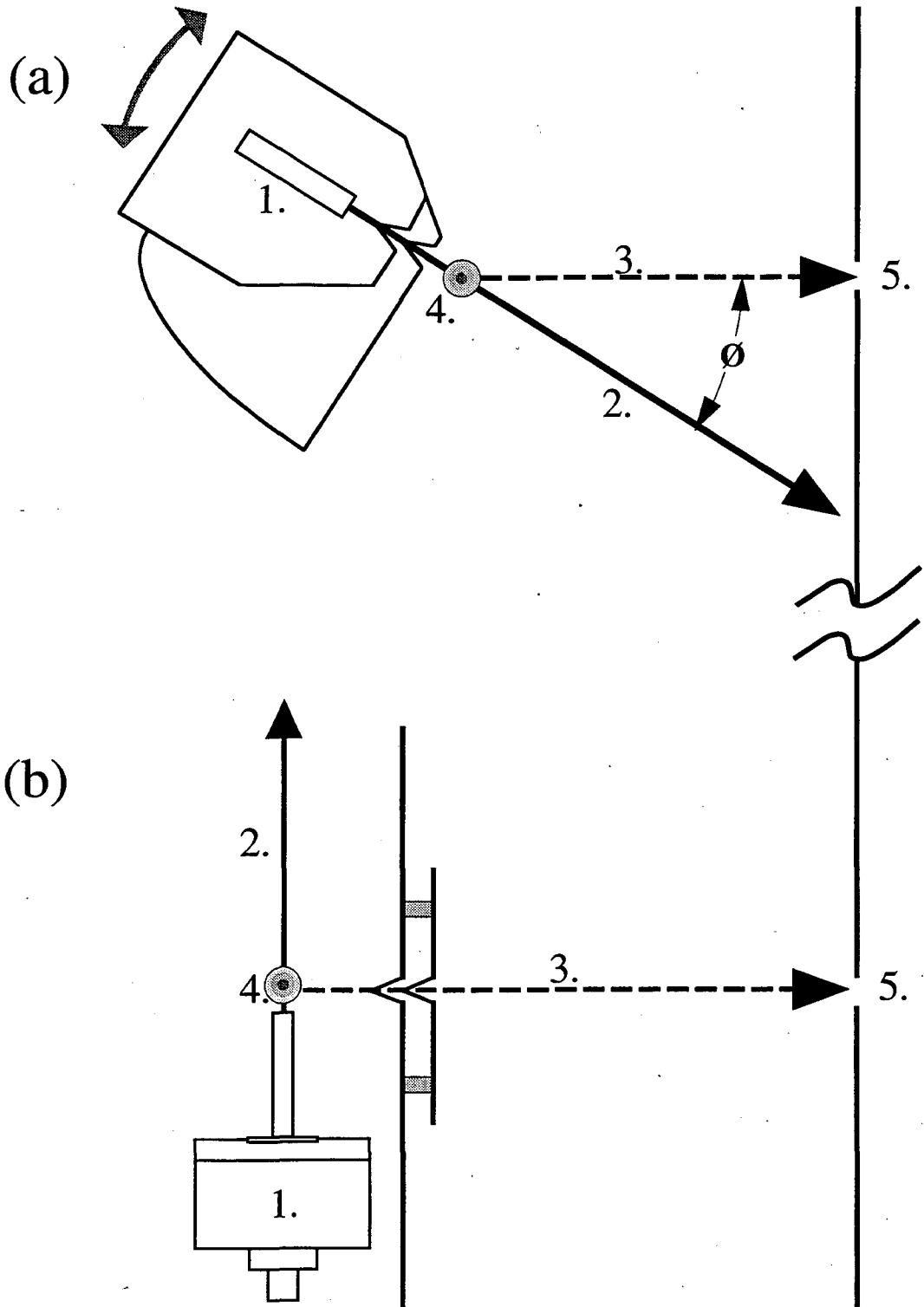


Figure 1

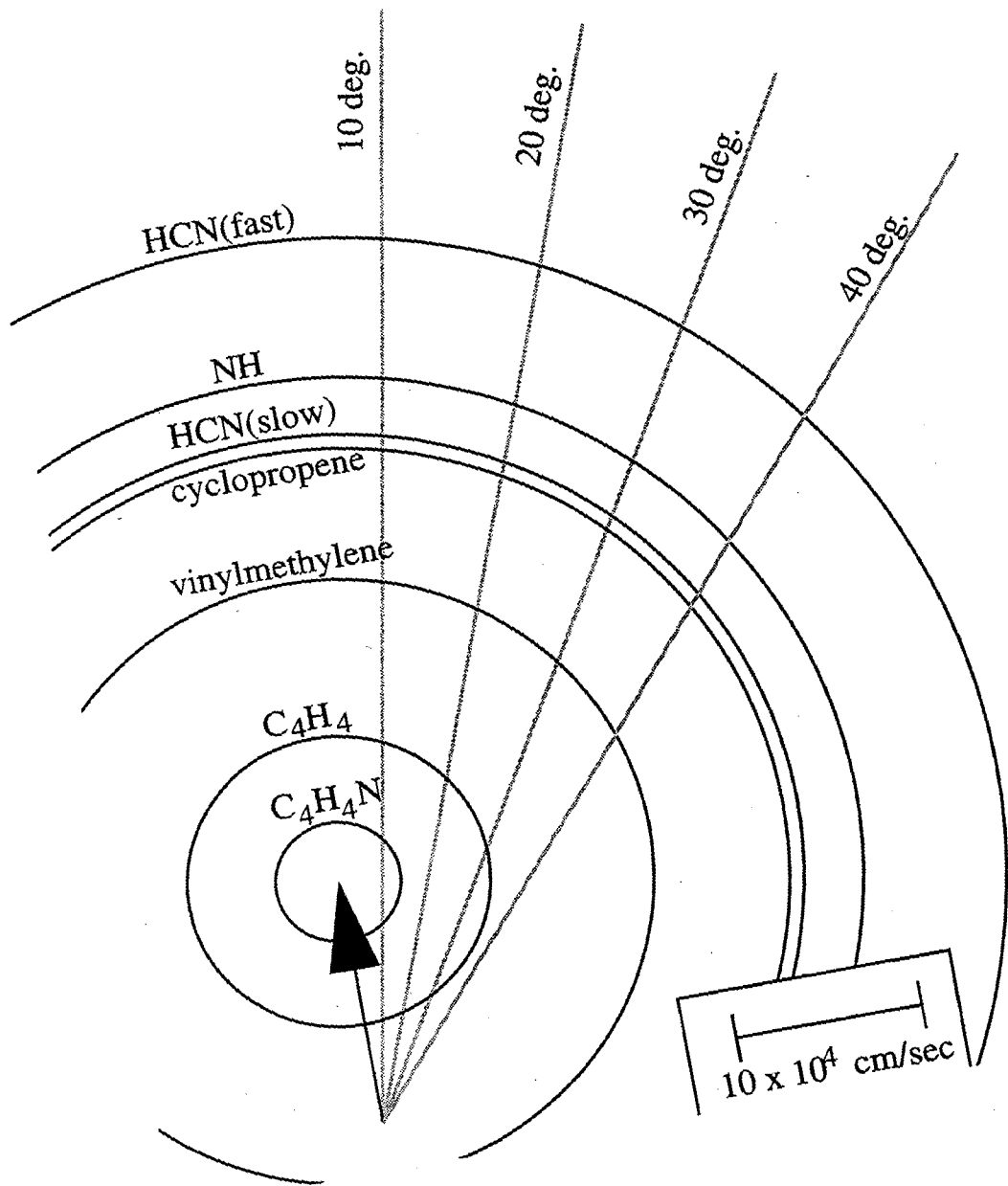


Figure 2

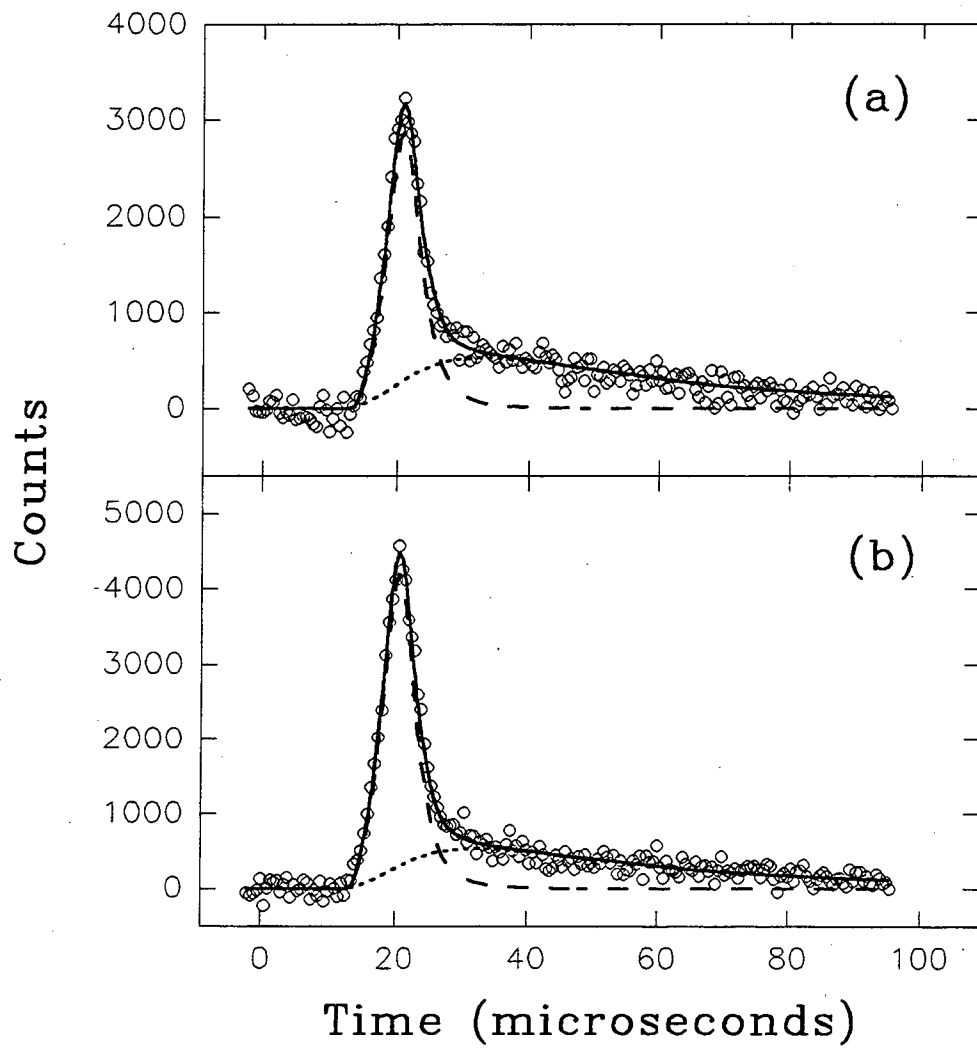


Figure 3

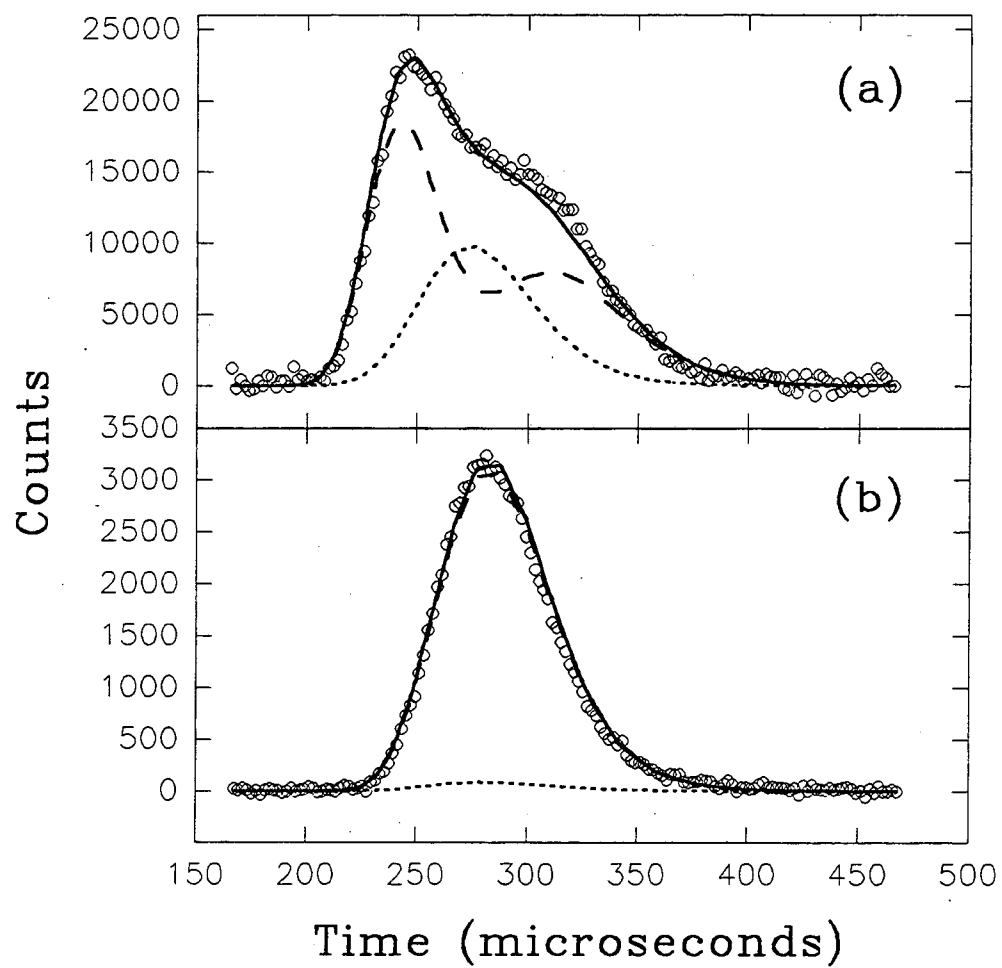


Figure 4

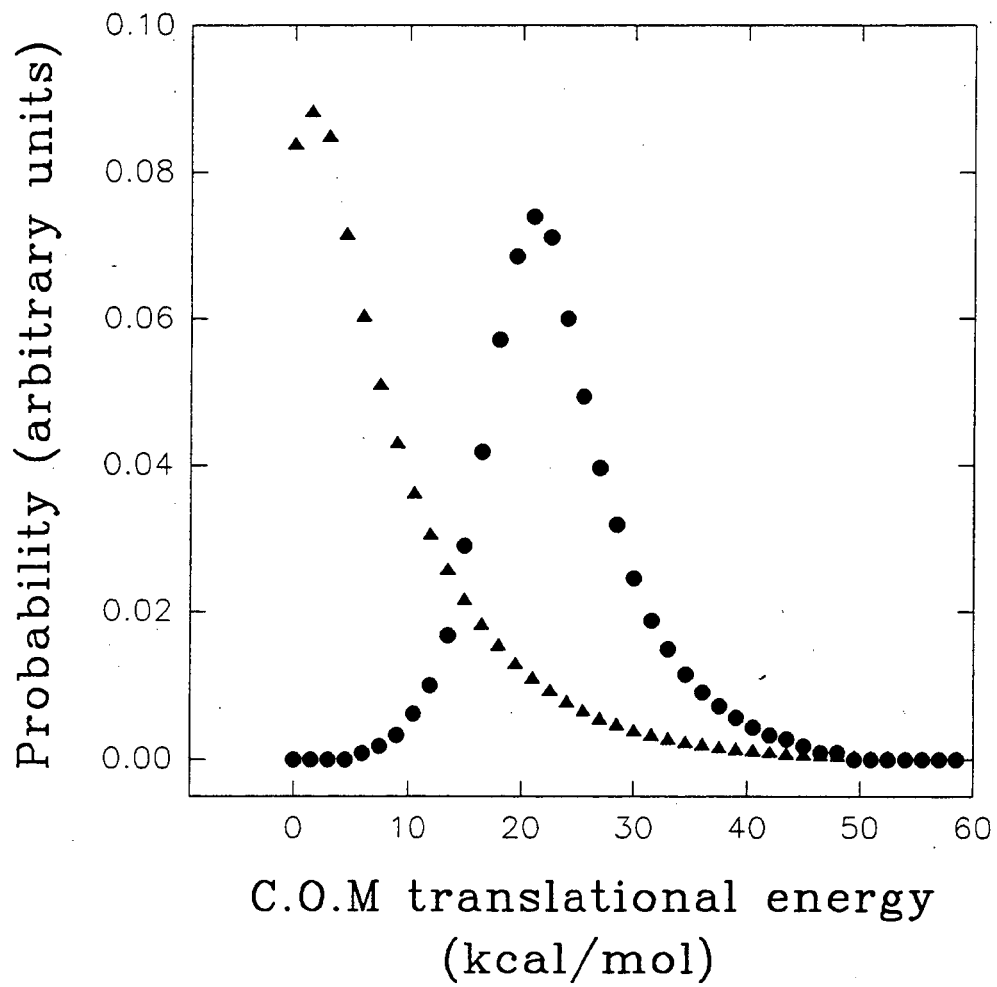


Figure 5

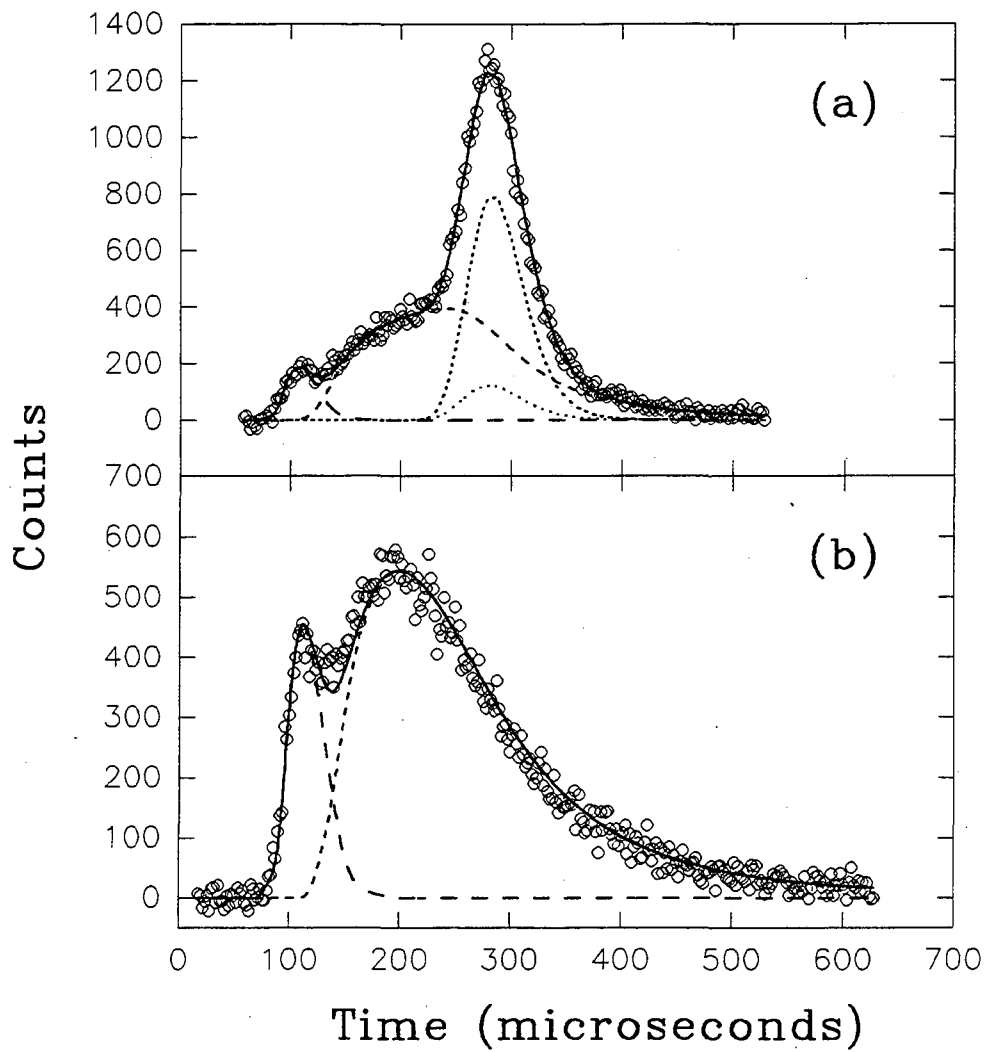


Figure 6

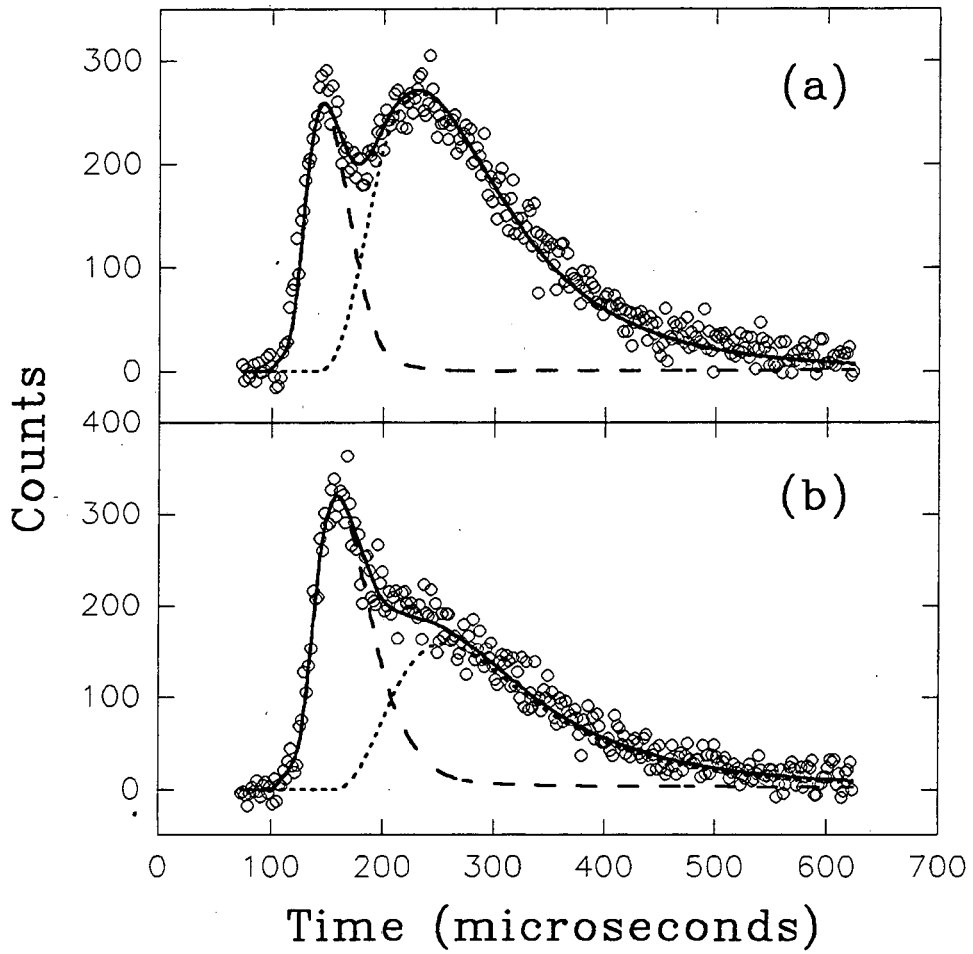


Figure 7

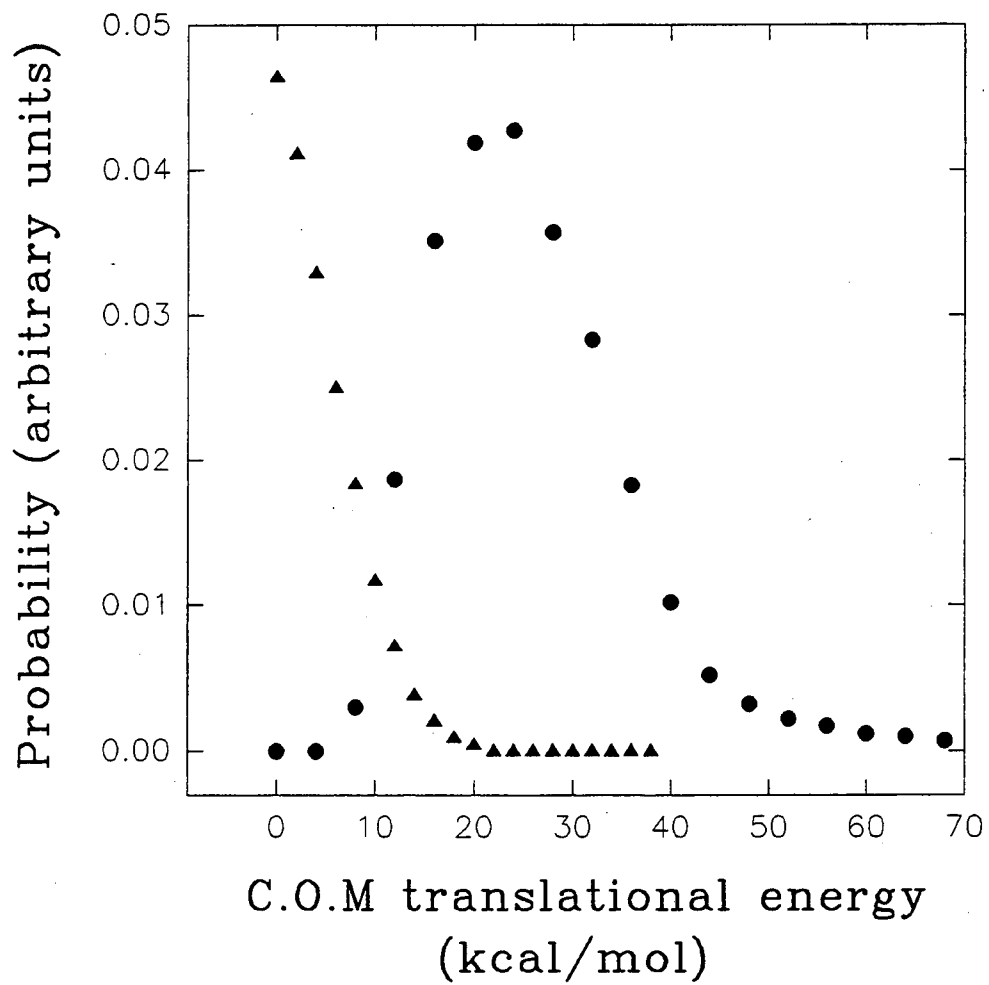


Figure 8

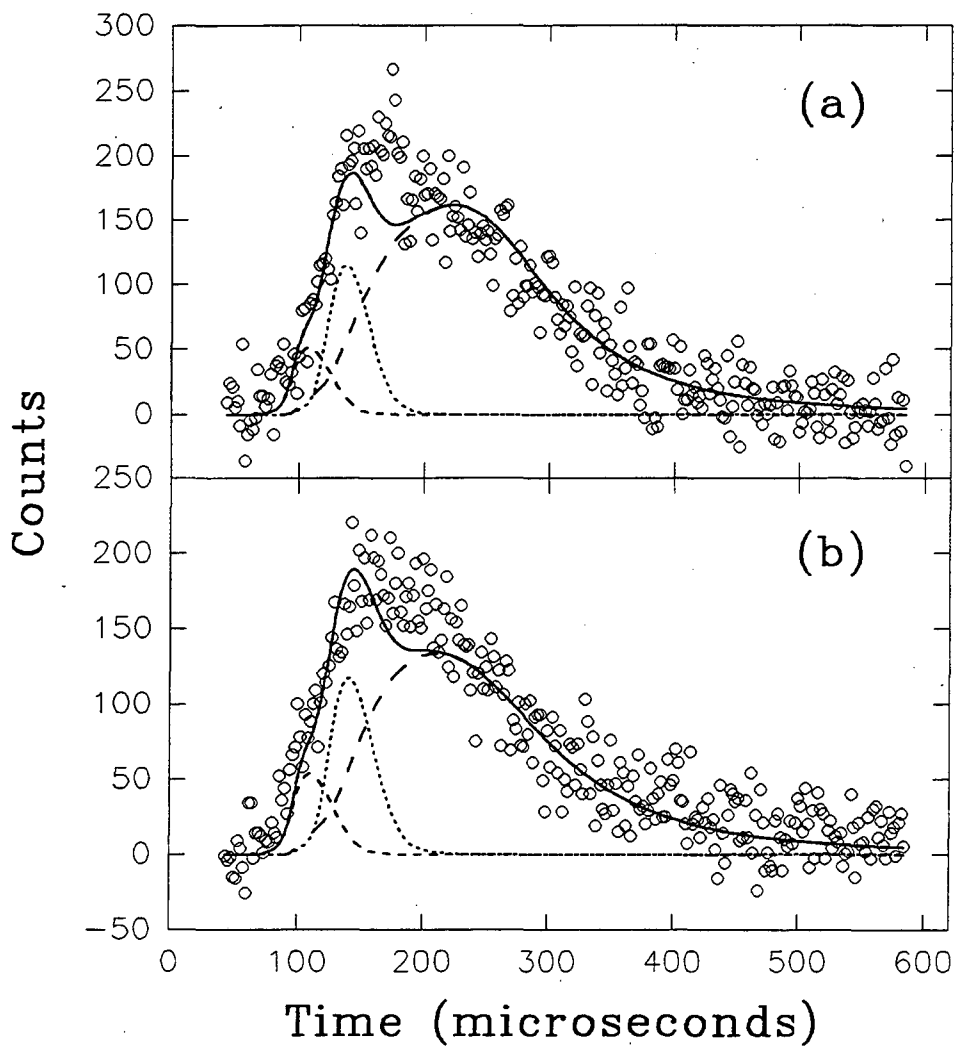


Figure 9

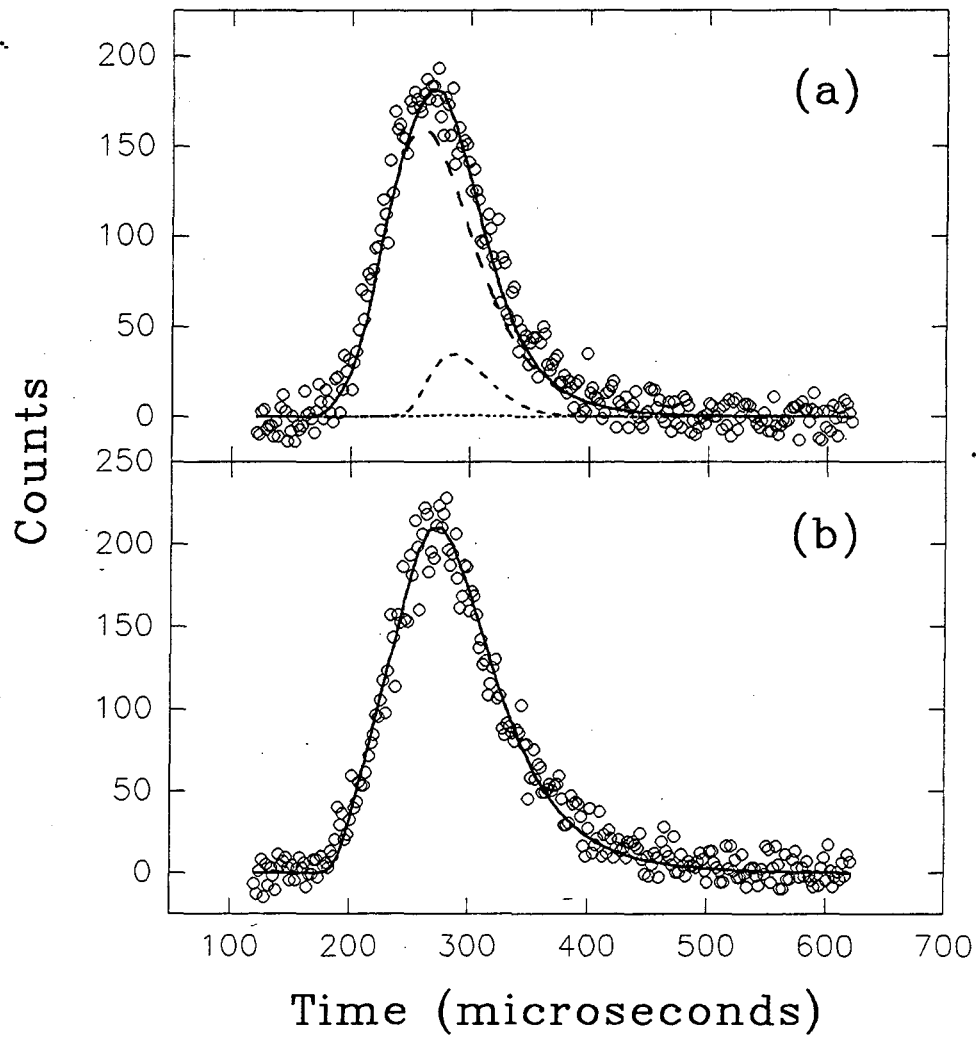


Figure 10

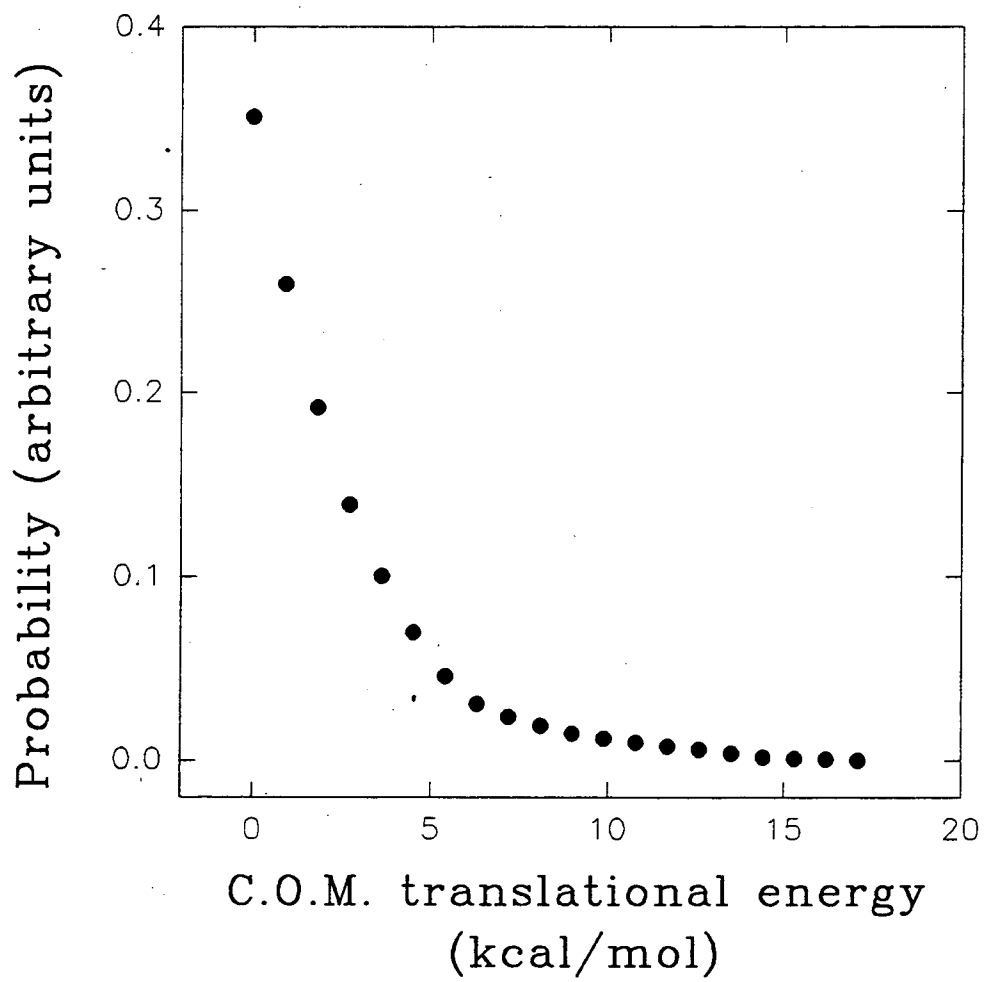


Figure 11

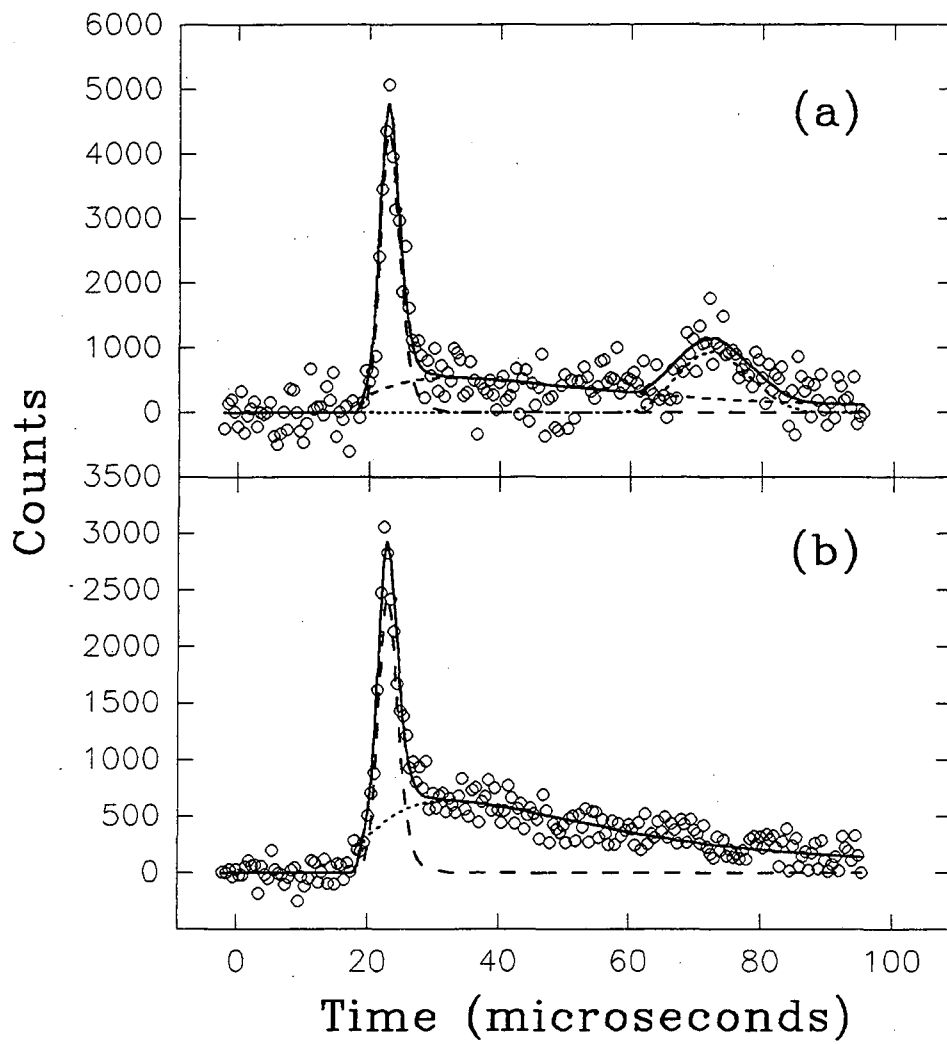


Figure 12

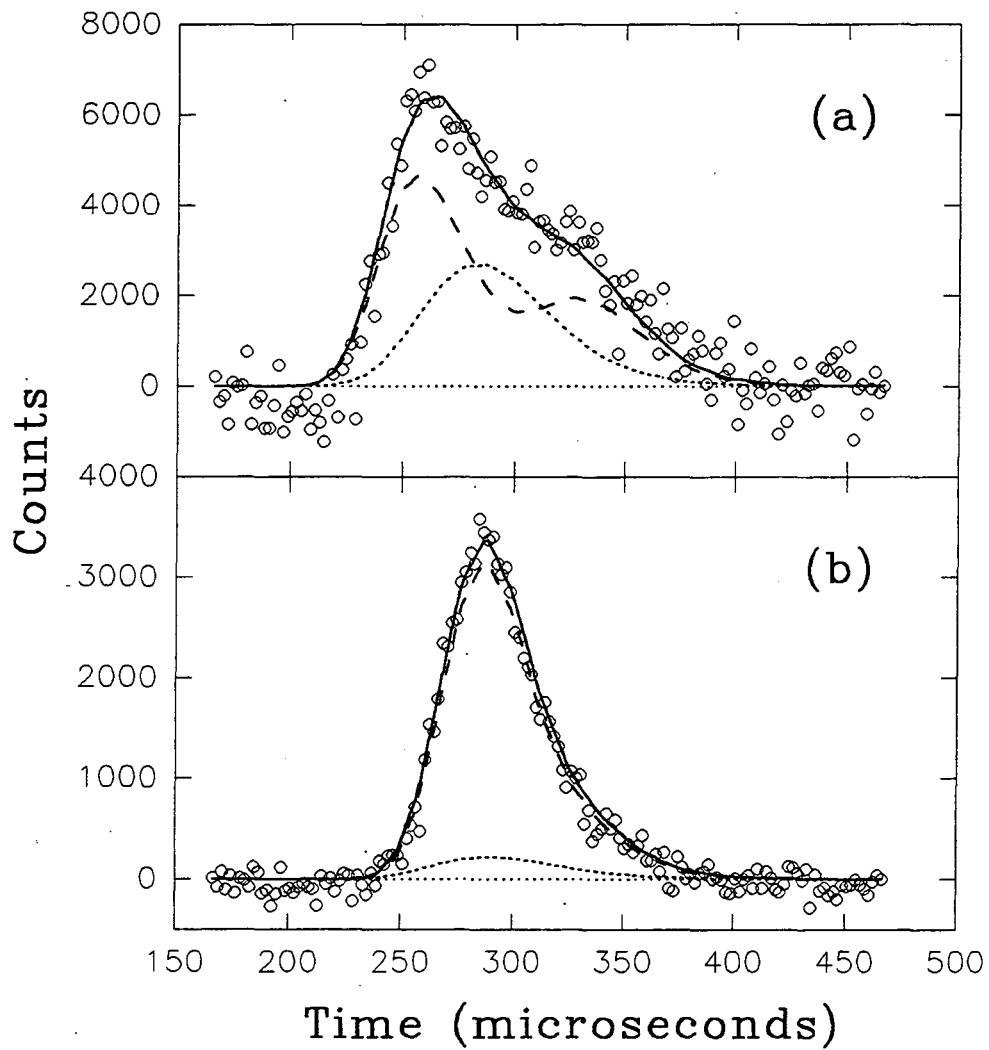


Figure 13

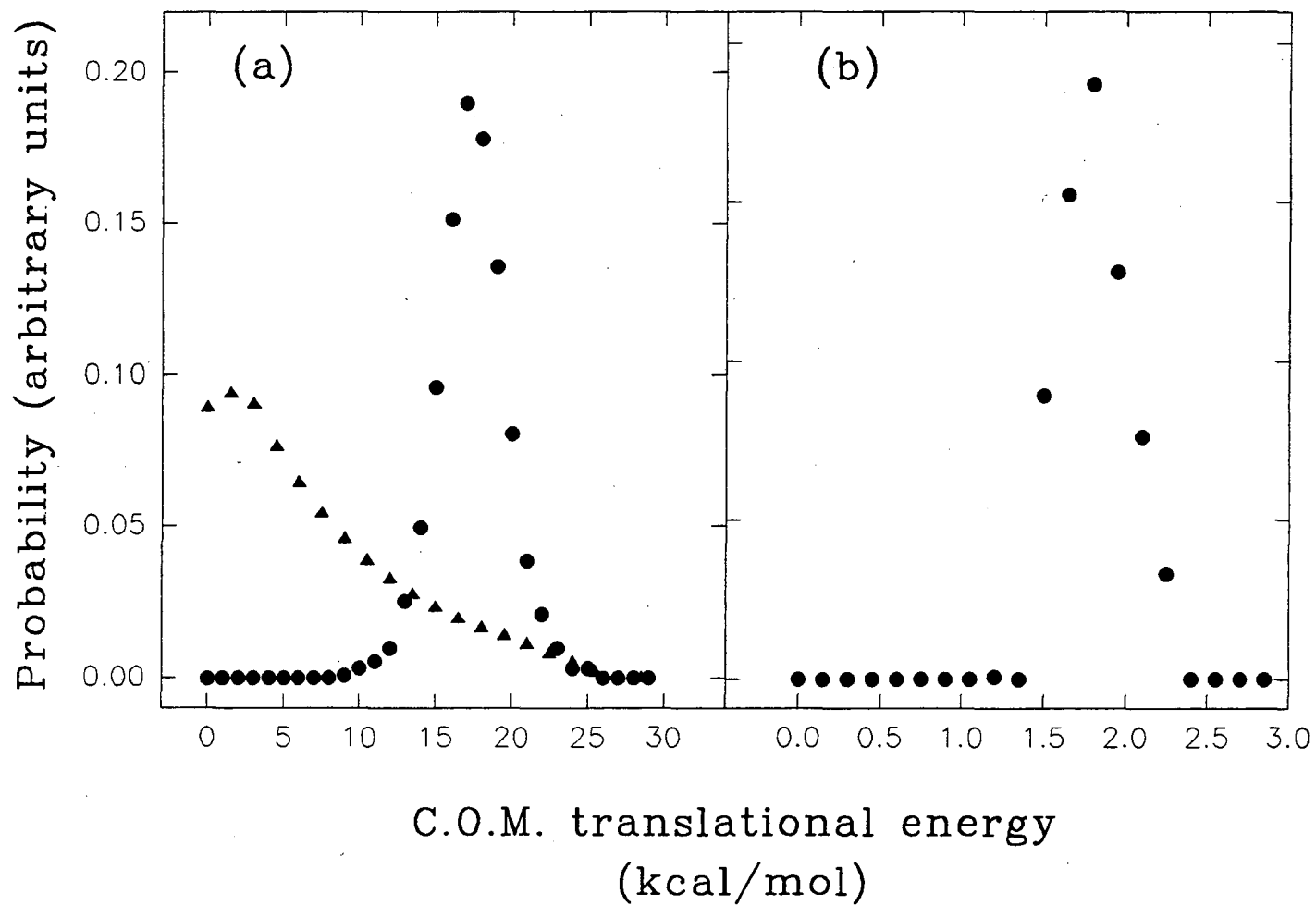


Figure 14

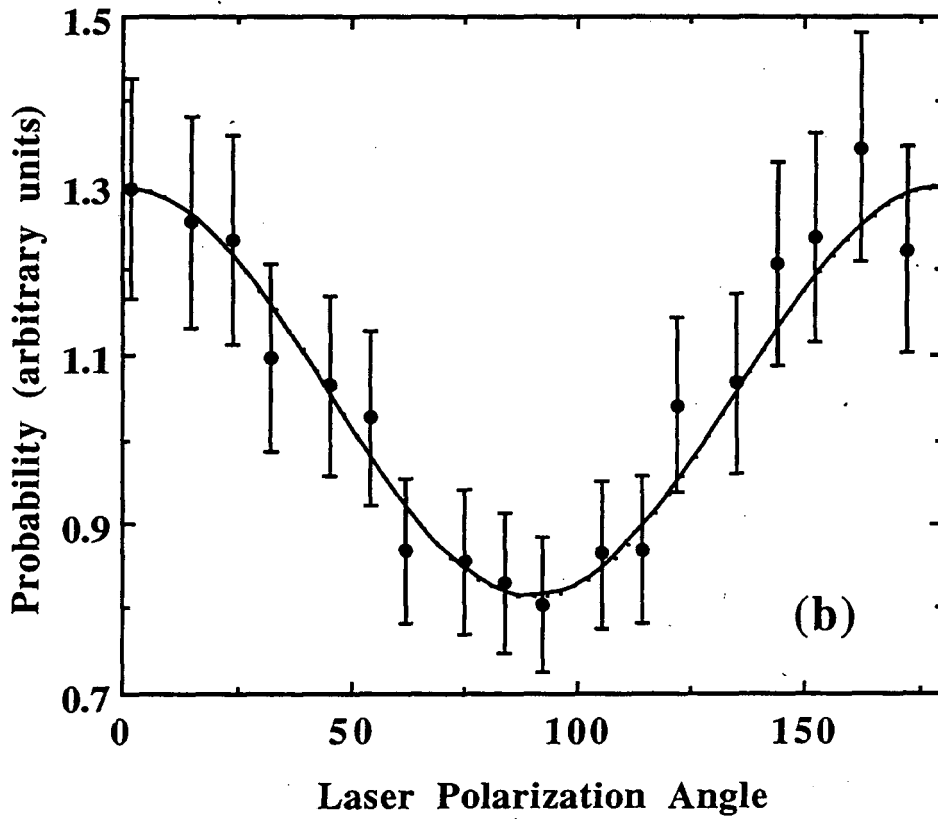
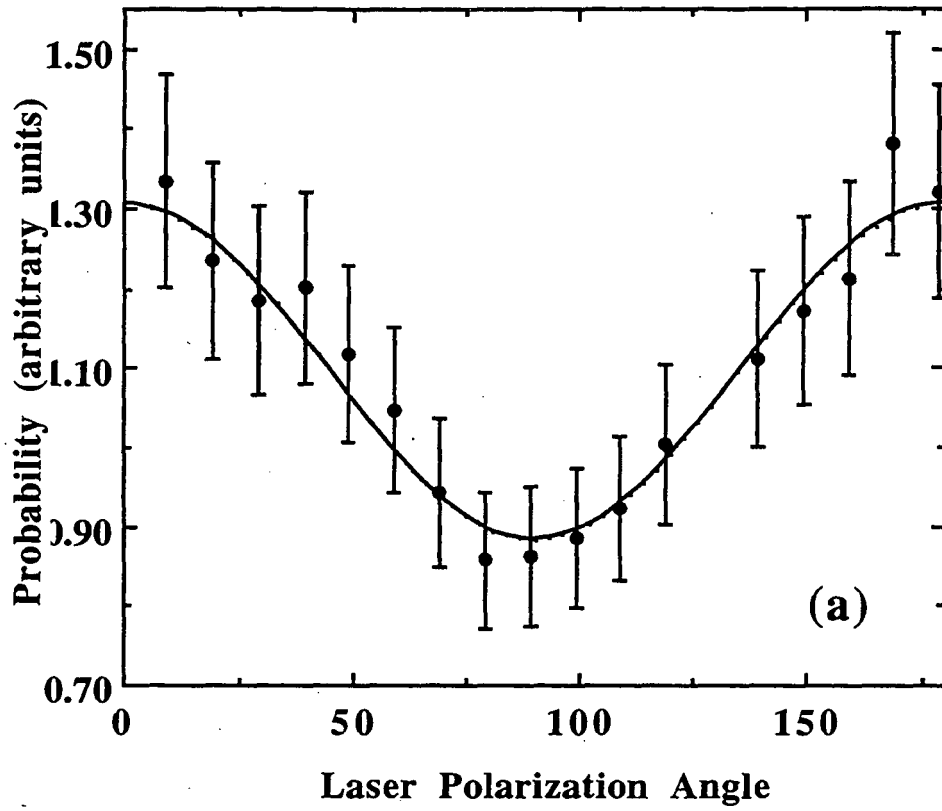


Figure 15

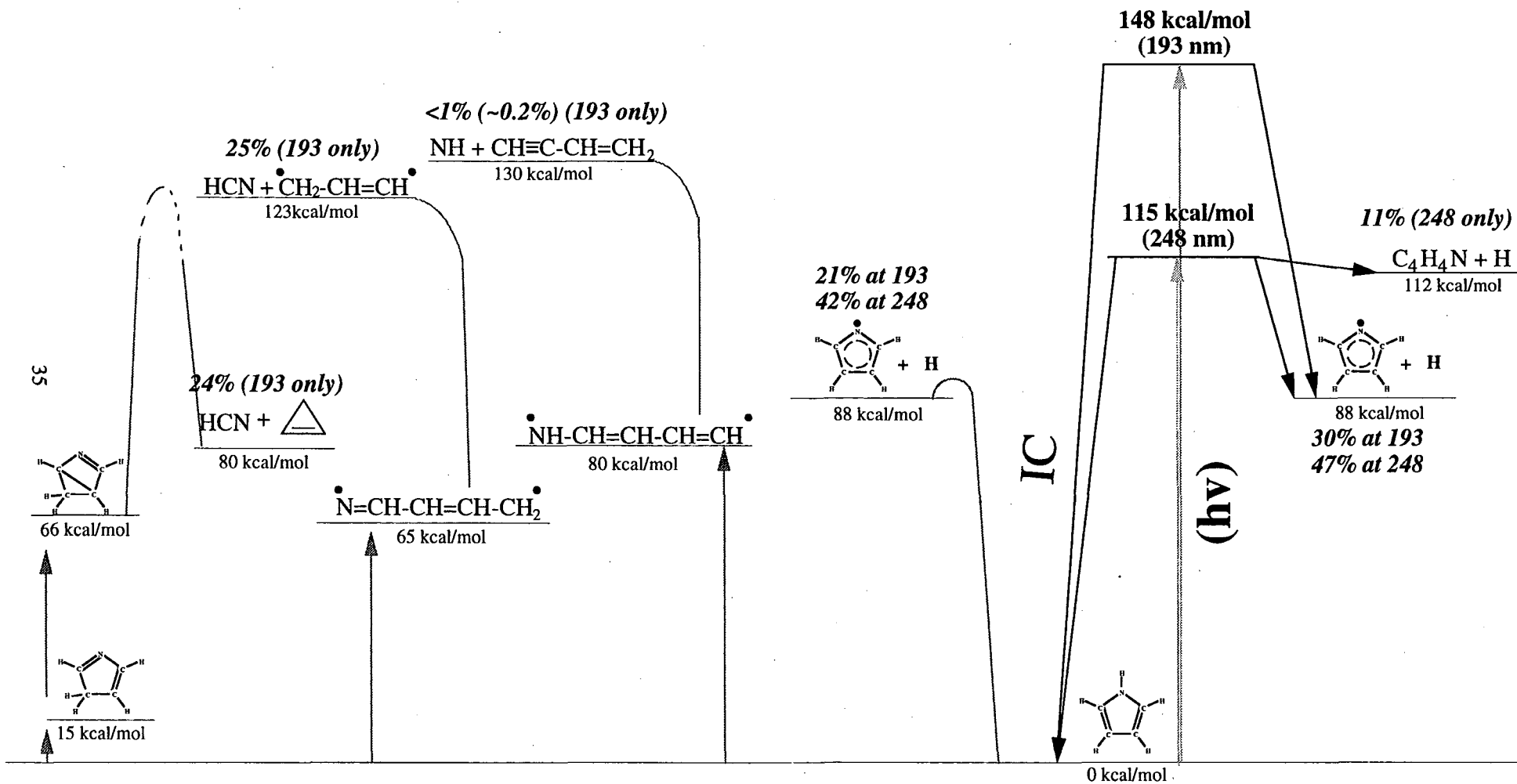


Figure 16

LAWRENCE BERKELEY LABORATORY
UNIVERSITY OF CALIFORNIA
TECHNICAL INFORMATION DEPARTMENT
BERKELEY, CALIFORNIA 94720